Journal of Catalysis 405 (2022) 641–651

Contents lists available at ScienceDirect

Journal of Catalysis

journal homepage: www.elsevier.com/locate/jcat

Deactivation and regeneration of solid acid and base catalyst bodies used in cascade for bio-oil synthesis and upgrading

Ana M. Hernández-Giménez [a], Héctor Hernando [b], Rosa M. Danisi [a,c], Eelco T.C. Vogt [a], Klaartje Houben [d], Marc Baldus [d], David P. Serrano [b], Pieter C.A. Bruijnincx [a,e,*], Bert M. Weckhuysen [a,*]

[a] Inorganic Chemistry and Catalysis, Debye Institute for Nanomaterials Science, Utrecht University, Universiteitsweg 99, 3584 CG Utrecht, the Netherlands
[b] Thermochemical Processes Unit, IMDEA Energy Institute, 28935, Móstoles, Madrid, Spain
[c] Institute of Applied Geosciences-Technical Petrophysics, Karlsruhe Institute of Technology, Adenauerring 20b, 76131 Karlsruhe, Germany
[d] NMR Spectroscopy, Bijvoet Center for Biomolecular Research, Department of Chemistry, Utrecht University, Padualaan 12, 3584 CH Utrecht, the Netherlands
[e] Organic Chemistry and Catalysis, Debye Institute for Nanomaterials Science, Utrecht University, Universiteitsweg 99, 3584 CG Utrecht, the Netherlands

ARTICLE INFO

Article history:
Received 8 May 2021
Revised 29 August 2021
Accepted 26 September 2021
Available online 4 October 2021

Keywords:
Catalytic fast pyrolysis
Bio-oil upgrading
Catalyst bodies
Coke formation
Structural damaging
Catalyst regeneration

ABSTRACT

The modes of deactivation -and the extent to which their properties can be restored- of two catalyst bodies used in cascade for bio-oil synthesis have been studied. These catalysts include a solid acid granulate (namely ZrO_2/desilicated zeolite ZSM-5/attapulgite clay) employed in *ex-situ* catalytic fast pyrolysis of biomass, and a base extrudate (K-exchanged zeolite USY/attapulgite clay) for the subsequent bio-oil upgrading. Post-mortem analyses of both catalyst bodies with Raman spectroscopy and confocal fluorescence microscopy revealed the presence of highly poly-aromatic coke distributed in an egg-shell manner. Deactivation due to coke adsorption onto acid sites affected the zeolite ZSM-5-based catalyst, while for the base catalyst it is structural integrity loss, resulting from KOH-mediated zeolite framework collapse, the main deactivating factor. A hydrothermal regeneration process reversed the detrimental effects of coke in the acid catalyst, largely recovering catalyst acidity (~80%) and textural properties (~90%), but worsened the structural damage suffered by the base catalyst.

1. Introduction

The production of fuels, such as bio-kerosene for aviation transportation, directly from lignocellulosic biomass is of increasing interest for energy sustainability [1]. Unfortunately, bio-oil produced via thermal pyrolysis of biomass does not meet the requirements desired for a transportation fuel as it is very viscous, dense, corrosive and poorly energetic [2]. Therefore, the bio-oil formed is required to undergo a set of upgrading steps, in which the energetic value is increased by oxygen depletion and by chain elongation. Catalytic fast pyrolysis (CFP) takes place at high temperatures (~500 °C), in an inert atmosphere (i.e., in the absence of oxygen) and with short residence times (i.e., few seconds) to lower the bio-oil oxygen content [3]. When CFP is performed in the so-called *ex-situ* mode [4], the catalyst is only contacted with the pyrolysis vapors after conducting the thermal pyrolysis step in a separate reactor. This way of operation favors the formation of aliphatics and olefins over aromatics, which are more interesting for bio-oil production. The bio-oil generated by *ex-situ* CFP can be further upgraded to advanced bio-fuels by subsequent deoxygenation reactions.

Traditionally, zeolite ZSM-5 has been mostly used for the CFP step. This can be done solely with zeolite ZSM-5 as the active phase [5,6] or in combination with promoters, such as Ni or Ga [7,8], which boost its efficiency in obtaining a high-quality deoxygenated bio-oil. The good activity of zeolite ZSM-5 is related to its shape selectivity, acidity and thermal stability [5,6]. However, a common limitation of zeolite ZSM-5 in the CFP process is its deactivation due to coke formation, which results in clogging its micropores. Creating mesoporosity within zeolite ZSM-5, e.g. via desilication [9], can considerably lower the detrimental effects of pore blockage by coke formation [10]. It is important to note that the formation of coke deposits is induced by olefin polymerization [11], as well as other C-C coupling reactions, all of which can abundantly occur during biomass conversion processes. C-C coupling reactions are also required, however, as part of the necessary bio-oil upgrading, with ketonization [12,13] or aldol condensation [14,15] being typical examples, given the large amounts of carboxylic acids, ketones

* Corresponding authors.
E-mail addresses: p.c.a.bruijnincx@uu.nl (P.C.A. Bruijnincx), b.m.weckhuysen@uu.nl (B.M. Weckhuysen).

https://doi.org/10.1016/j.jcat.2021.09.029
0021-9517/

and aldehydes present in bio-oil [16]. Indeed, these reactions are often the topic of (model) bio-oil upgrading and deoxygenation studies and are commonly catalyzed by base catalysts, such as metal oxides (e.g., ZrO_2, TiO_2 or hydrotalcites) or alkali metal-exchanged zeolites [17,18].

For bench-scale and pilot-scale testing, the use of shaped catalyst bodies is required to ensure mechanical strength and to avoid pressure drop issues in the chemical reactors used [19]. To make suitably shaped catalyst bodies, binder materials, such as clay minerals and alumina, are typically added to the powdered catalysts to obtain a mixture that upon extrusion or granulation generates the shaped catalyst bodies. However, binders can modify the catalyst properties and hence activity, e.g. by offering a source of metal cations that can exchange with and alter the catalyst's active sites, altering for example catalyst acidity within a zeolite [20,21]. Yet, binder materials can also affect the catalyst's stability. Deactivation of catalyst bodies has been studied, for instance, for fluid catalytic cracking (FCC) particles. These FCC particles are formed via e.g., a spray drying procedure of the different catalyst components and consist of a zeolite material, e.g. zeolite H-Y, promoted or not with active metals (e.g., La), binder and filler materials, such as SiO_2, Al_2O_3 and clay minerals [22,23]. The binder and filler materials improve the stability of the active zeolite component, which would suffer from more structural damage under the hydrothermal conditions applied in the industrial reactor and regenerator systems if the binder and filler would not be present [24]. Common reasons for FCC catalyst deactivation are poisoning by coke [25,26] and metals deposition which leads to catalyst particle agglutination, impeded accessibility of the zeolite's pore network, and alterations in size and acidity, as illustrated by Meirer et al. [27–29].

The nature of the binder material in a catalyst body has a significant impact on its performance. On extruded zeolite-based catalysts, Verkleij et al. reported on the higher resistance against deactivation for zeolite ZSM-5 when blended with Al_2O_3 rather than SiO_2, in the 1-hexene oligomerization reaction. Indeed, the Al_2O_3-based system better favored elongated oligomers over branched ones, protecting the zeolite pores better against clogging [30]. The same catalyst systems, when applied in the transalkylation of aromatics [31,32], also showed differences in stability. In this case, the Al_2O_3-based catalyst extrudates showed more and more condensed coke deposits than the SiO_2-based catalyst. These deposits were located mainly on the rim of the zeolite crystals, however, while in the case of the SiO_2-based catalyst extrudates coke deposits could be found throughout the zeolite crystals, leading to faster deactivation.

Indeed, the choice of the binder and its integration with the other components of the technical catalyst – i.e., the manner in which e.g. porosity, crystal size or acidity of the zeolite component is affected - will impact the mode, rate and extent of catalyst deactivation, as previously reported [33]. To reverse (totally or partially) certain causes of catalyst deactivation, oxidative regeneration cycles at high reaction temperatures can be carried out [34,35]. Indeed, by burning-off the coke deposits from spent catalysts, pore or active site blockage can in principle be reversed and the physicochemical properties of the catalyst material, such as surface area, pore volume and acidity, restored. As an example, Michels et al. demonstrated that upon regeneration in flowing air at 550 °C for 3 h, a zeolite ZSM-5-based catalyst extruded with attapulgite as binder material showed a significant recovery of the textural properties and catalytic activity in the methanol-to-hydrocarbons (MTH) reaction [36]. However, other causes of catalyst deactivation, such as morphological and textural changes, could not be repaired by such a regeneration process. Indeed, because of the high temperatures and steam generated upon coke combustion, changes in the structural and textural properties of the catalyst usually worsen [25]. In line with this observation, previous reports [37] emphasized the importance of applying intermediate regeneration temperatures (yet equal or higher than the reaction temperature), to ensure total combustion of the coke deposits formed within the zeolite catalyst but avoid irreversible structural damages.

In this work, we report on the different modes of deactivation of two tailored catalysts used in cascade for a more efficient bio-oil deoxygenation in lignocellulose catalytic pyrolysis. This cascade reaction [38] combines the synergistic effect of a solid acid ZrO_2/desilicated zeolite ZSM-5/attapulgite clay mineral (further denoted as ZrO_2/ds-ZSM-5-ATP) -employed for the *ex-situ* CFP step- and a solid base K-grafted zeolite USY/attapulgite (further denoted as K-(USY-ATP)) -used in the subsequent bio-oil upgrading step-. While the acidity of the ZSM-5-based catalyst is key to promote cracking and alkylation reactions involved within the catalytic pyrolysis stage, the basicity of the alkaline-grafted USY catalyst is so for the subsequent upgrading of bio-oil via deoxygenating routes, such as aldol condensations [15].

Understanding the origin and cause of the deactivation of these catalysts, as well as the extent to which deactivation can be reversed by a suitable regeneration treatment will allow optimizing the catalyst lifetime. To this extent, the catalyst materials were extensively characterized using bulk and spatially-resolved characterization techniques on fresh, spent and regenerated samples in their shaped form. The extent, nature and location of coke formation, the structural integrity and acid/base properties of the catalyst materials, and the regeneration effects on coke removal and recovery of the original properties have been assessed.

2. Experimental

The experimental details related to catalysts syntheses and characterization are presented in the Supporting Information.

2.1. Cascaded catalytic bio-oil production

The bench scale set-up in which ZrO_2/ desilicated ZSM-5-attapulgite catalyst (ZrO_2/ds-ZSM-5-ATP) as solid acid and K-exchanged zeolite USY/attapulgite catalyst (K-(USY-ATP)) as solid base were tested is schematically depicted in Fig. 1c [39]. Biomass feedstock consisted of previously de-ashed wheat straw (4 g) heated to 550 °C and fluidized in 100 NmL/min N_2. In a first stage, a catalytic bed of ZrO_2/ds-ZSM-5-ATP is exposed to the pyrolytic vapors coming from the thermal pyrolysis stage. The subsequent stage consists of a fixed bed of K-(USY-ATP) catalyst for the for the treatment of the catalytic vapors, which are further upgraded. Both catalytic pyrolysis and upgrading processes operate at 450 °C, and on both processes the catalyst to biomass ratio (C/B) was of 0.6 (excluding the binder into the catalyst weight). The vapors leaving the reactor were condensed to collect the liquid bio-oil for approx. 10 min; non-condensable gases were collected in sampling bags at the end of the line. The energy yield associated with bio-oil product was calculated as the proportion of chemical energy (HHV) retained regarding that of raw biomass.

2.2. Regeneration process

Regeneration of both catalysts was carried out under static air by heating the catalyst bodies in an open crucible at a temperature ramp of 1.8 °C/min up to 550 °C and holding this temperature for 6 h.

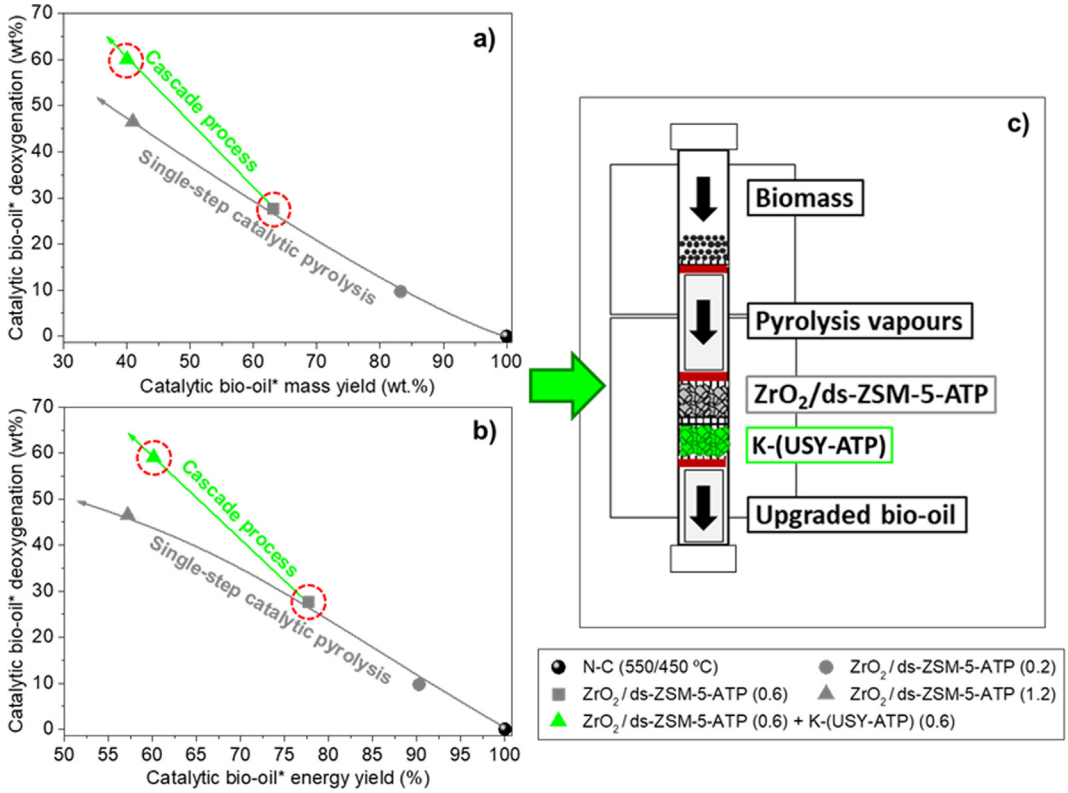

Fig. 1. Bio-oil catalytic deoxygenation vs catalytic mass (a) and energy yields (b), for non-catalytic and single and cascade catalytic pyrolysis experiments, using the thermal bio-oil as calculation basis, and schematic experimental set-up (c).

3. Results

3.1. Catalyst performance

Fig. 1 shows the activity of the cascade process, consisting of an *ex-situ* catalytic fast pyrolysis step (i.e., thermal and catalytic pyrolysis) with a ZrO_2/ desilicated ZSM-5-attapulgite catalyst (ZrO_2/ds-ZSM-5-ATP) as solid acid and a catalytic upgrading step with a K-exchanged zeolite USY/attapulgite catalyst (K-(USY-ATP)) as solid base. The activity is expressed as the catalytic bio-oil deoxygenation as a function of the mass yield (a) and the energy yield (b) for the cascade process (see reactor scheme in Fig. 1c) compared to the single-step CFP process run with ZrO_2/ds-ZSM-5-ATP only.

After applying this three-step cascade process for a catalyst/biomass (C/B) ratio of 0.6, and for a bio-oil mass yield of 40 wt%, the deoxygenation degree (compared to the non-catalytic thermal bio-oil) was ~60 wt% (see green triangle data in Fig. 1a). For the *ex-situ* CFP only experiment, the run with a C/B ratio adjusted at 1.2 to run at equal total amount of catalyst material used. The deoxygenation degree was ca. 15 wt%, clearly inferior to the cascade catalytic process (grey triangle data series). Also, it turned out that at the same weight conditions the energy yield (Fig. 1b) is higher when two catalytic processes are coupled (60%) with respect to only one catalytic step (57%). Accordingly, the cascade process leads to both enhanced bio-oil deoxygenation and energy yield.

3.2. Catalyst deactivation

3.2.1. Type of coke deposits

After *ex-situ* CFP, 6.8 wt% of coke was formed in the ZrO_2/ds-ZSM-5-ATP catalyst, as determined by thermogravimetric analysis-mass spectrometry (TGA-MS) (Fig. S1). The main part of it (6.0 wt%) was highly deficient in hydrogen, indicated by the high temperature of combustion (~480 °C, Fig. S1a-b) [40]. Given the likely insoluble character of the coke formed which precludes the analysis by chromatography, its polyaromatic nature was confirmed by FT-IR spectroscopy, showing the characteristic stretching bands of condensed ring aromatic structures ($\nu_{C=C}$) in the 1560–1600 cm^{-1} spectral region and the C-H stretching vibrations (ν_{CH}) corresponding also to aromatic coke at 3067 cm^{-1} with contributions of methylene (2930 and 2860 cm^{-1}) and methyl (2970 cm^{-1}) groups [41] (Fig. S2a). Condensations, alkylations and isomerization reactions produced upon CFP may be responsible for the origin of these polyaromatic species. The FT-IR spectrum showed also signatures of aldehydes (ν_{CH} at 2745 cm^{-1}, $\nu_{C=O}$ at 1714 and 1691 cm^{-1}), olefins ($\nu_{C=C}$ 1636 cm^{-1}) and organic acids ($\nu_{C=O}/\nu_{O-H}$ 1616 cm^{-1}), among other compounds, indicating the presence of oxygenates in the carbon deposits including phenols and furans. The corresponding UV–Vis diffuse reflectance spectrum (Fig. S2b) further corroborated the aromatic nature of coke with the presence of species such as pyrenes (with absorption bands at ~250–350 nm) [42], naphthalenes and anthracenes (with absorption bands at ~280–400 nm) and more conjugated polyaromatic carbonaceous species and/or graphite-like coke, likely insoluble, characterized by absorption bands with maxima at >400 nm [43].

The size of the coke deposits formed on the spent ZrO_2/ds-ZSM-5-ATP catalyst was estimated by Raman spectroscopy, based on the expression introduced by Ferrari and Robertson for disordered graphitic carbons and graphene (see Eq. (1) in the Supporting Information) [44,45]. Based on the D and G integrals (Fig. S3a), the average coke size is estimated to be between 5 and 10 Å. Substituted pyrenes (Fig.S3b) are of this size and have been proposed by Guisnet and Magnoux as average component of the (soluble) coke formed within zeolite H-ZSM-5 material for a coke content close to 9 wt %, with an approximate boiling point close to 400 °C [46].

The spent K-(USY-ATP) catalyst extrudate, employed for the catalytic deoxygenation of the bio-oils formed in the first CFP step, showed a lower amount of coke deposits than the ZrO_2/ds-ZSM-5-ATP CFP catalyst. This is consistent with the process setup, with the zeolite ZSM-5-based catalyst being directly exposed to the raw pyrolytic vapors, while the K-loaded zeolite USY-based catalyst further upgrades the already treated vapors. TGA-MS analysis of the spent USY catalyst (Fig. S1c,d) showed a coke content of 5.6 wt%, being for the largest part again poly-aromatic [40] (4.9 wt%, combusting at ~415 °C), while a smaller fraction is attributed to hydrogen-richer coke (Table 1). The nature of the coke deposits was further characterized by FT-IR spectroscopy (Fig. S2c) and UV–Vis DRS (Fig. S2d). FT-IR spectroscopy on the spent K-(USY-ATP) catalyst material (Fig. S2c) showed the presence of aromatics (ν_{CH} at 3067 cm^{-1}) and coke ($\nu_{C=C}$ at 1574, 1600 cm^{-1}). As expected, the lower content of aromatics and coke for the K-(USY-ATP) catalyst was indicated by the lower relative intensities of these bands (Fig. S2c) compared to the ZSM-5-based catalyst employed in the first catalytic stage (a). It should be noted that the FT-IR bands at 2745 cm^{-1} (ν_{CH}) and 1714 cm^{-1} ($\nu_{C=O}$) are indicative of aldehydes, showing also oxygenates presence which originate from the deoxygenation activity carried out by the K-(USY-ATP) catalyst. The UV–Vis DRS spectrum of the spent K-(USY-ATP) catalyst material (Fig. S2d) indicates the presence of hydrogen-rich coke types, such as alkylated benzenes, absorbing light in the range of 250–270 nm; hydrogen-deficient coke types, such as naphthalenes and anthracenes, which absorb light in the range of 280–400 nm [43]; and poly-aromatic carbonaceous species above 400 nm.

3.2.2. Location of coke deposits

As catalyst extrudates might be subject to diffusion limitations, any coke deposits formed could be non-homogeneously distributed over the shaped catalyst body. To study any spatial distribution of the coke deposits, the spent technical catalysts were studied by Confocal Fluorescence Microscopy (CFM) [47], as schematically depicted in Fig. 2.

Visual inspection after cross-sectioning of the spent ZrO_2/ds-ZSM-5-ATP catalyst showed a clear egg-shell distribution of the coke deposits formed. When the surface/shell (Fig. 2a) was irradiated with the excitation lasers of the CFM set-up, no fluorescence could be detected because of the high amount of poly-aromatic or (even) coke, which renders the surface opaque. When moving from the edge to the center of the catalyst body (Fig. 2b), fluorescence was seen, where there were less coke deposits and of softer nature -i.e. H-richer- than on the catalyst surface. Distinguished regions can be observed: brighter ones (highlighted in red, labelled as 2) with an extensive presence of naphthalenes and anthracenes (emitting light at wavelengths below 550 nm), and darker (green, 3) with higher presence of poly-aromatics (with more than 3 aromatic rings) which emit light above 550 nm [47,48]. The ratio between poly-aromatic and anthracene-like carbonaceous species was more pronounced in the regions located closer to the edge of the cross-section, (3, green), confirming the higher presence of more conjugated coke on more external locations of the catalyst body.

Zooming in at a central position of the cross-section (1, blue, Fig. 2b and Fig. 2c) revealed various bright spots (A) assigned to the presence of zeolite crystals (0.5–2 μm) where coke preferentially forms in mesopore walls [49,50] given the high concentration of Brønsted acid sites for the zeolite ds-ZSM-5 [51]. By contrast, the darker spots (B) might correspond to the presence of attapulgite crystals (0.5 μm × 30 nm), which given their absence of Brønsted acid sites [52] would produce less coke deposits [53,54].

The spent K-(USY-ATP) catalyst extrudate showed an egg-shell distribution of coke deposits too, visually confirmed by the gradient in color over the extrudate cross-section (Fig. S4). Indeed a larger proportion of poly-aromatics [47,48,55] was found on the external surface, while inner spots of the catalyst extrudate contained more coke rich in hydrogen (mainly naphthalenes/anthracenes emitting light between 400 and 500 nm). The shell, with an approximate thickness of ½ mm, was better distinguished when recording spectra on selected spots/regions due to the lower fluorescence intensity compared to the core of the section (Fig. 2d). The catalyst extrudate's surface (Fig. 2a) also contained regions of higher fluorescence intensity presenting a similar concentration profile as seen in the core of the cross-section, which is possibly associated with local attapulgite agglomeration. Note that for this catalyst material the unique source of (very weak) Brønsted acid sites is the clay mineral given that the zeolite USY is highly dealuminated (i.e., a Si/Al ratio of ~400) [56].

3.2.3. Changes in textural properties

The influence of coke deposits and their subsequent regeneration on the textural properties of spent and regenerated catalyst bodies were determined by physisorption of Ar gas at −196 °C. The results are shown in Fig. S5 and summarized in Table 1.

The ZrO_2/ds-ZSM-5-ATP catalyst, which showed a type I to type IIb isotherm with a steep H3 hysteresis loop [57,58] when fresh, (Fig. S5a, associated with a microporous material with additional mesoporosity) changed to a type I isotherm with a flatter H4 hysteresis loop after reaction. This was caused by the big loss in micropore and, in particular mesopore volume, partially blocked by the formation of coke deposits. The surface area was also significantly reduced after reaction (~38% in drop, Table 1). The pore-size distributions plot (Fig. S5b) reveals that the micropores (filled at low relative pressures) and mesopores (filled at higher relative pressures) were partially shuttered after reaction. Notably, with the regeneration procedure applied the original textural properties were recovered to a large extent (up to ~92%) with micro- and mesoporosity, as indicated in Table 1.

Table 1
Overview of the textural and acidic properties of the ZrO_2/ds-ZSM-5-ATP and K-(USY-ATP) technical catalysts in their fresh, spent and regenerated state.

	ZrO_2/ds-ZSM-5-ATP			K-(USY-ATP)		
Sample	Fresh	Spent	Regenerated	Fresh	Spent	Regenerated
BET (m^2/g)	263	164	242	472	406	455
S_{ext} (m^2/g)	86	50	85	388	337	382
S_{micro} (m^2/g)	177	114	157	84	69	73
V_{micro} (cm^3/g)	0.068	0.044	0.060	0.177	0.134	0.152
V_{meso} (cm^3/g)	0.164	0.085	0.157	0.148	0.074	0.085
Coke (wt.%)	–	6.8	–	–	5.6	–
Acidity (μmol/g)[a]	180 (BAS + LAS)	86 (BAS + LAS)	146 (BAS + LAS)	15 (LAS)	LAS	14 (LAS)
Basicity (μmol/g)[b]	n.a.	n.a.	n.a.	244	71	42

[a] Determined by FT-IR spectroscopy with pyridine as probe molecule (see Fig. 3b). LAS = Lewis acid sites, BAS = Brønsted acid sites. n.a = not analyzed.
[b] Determined by CO_2-TPD.

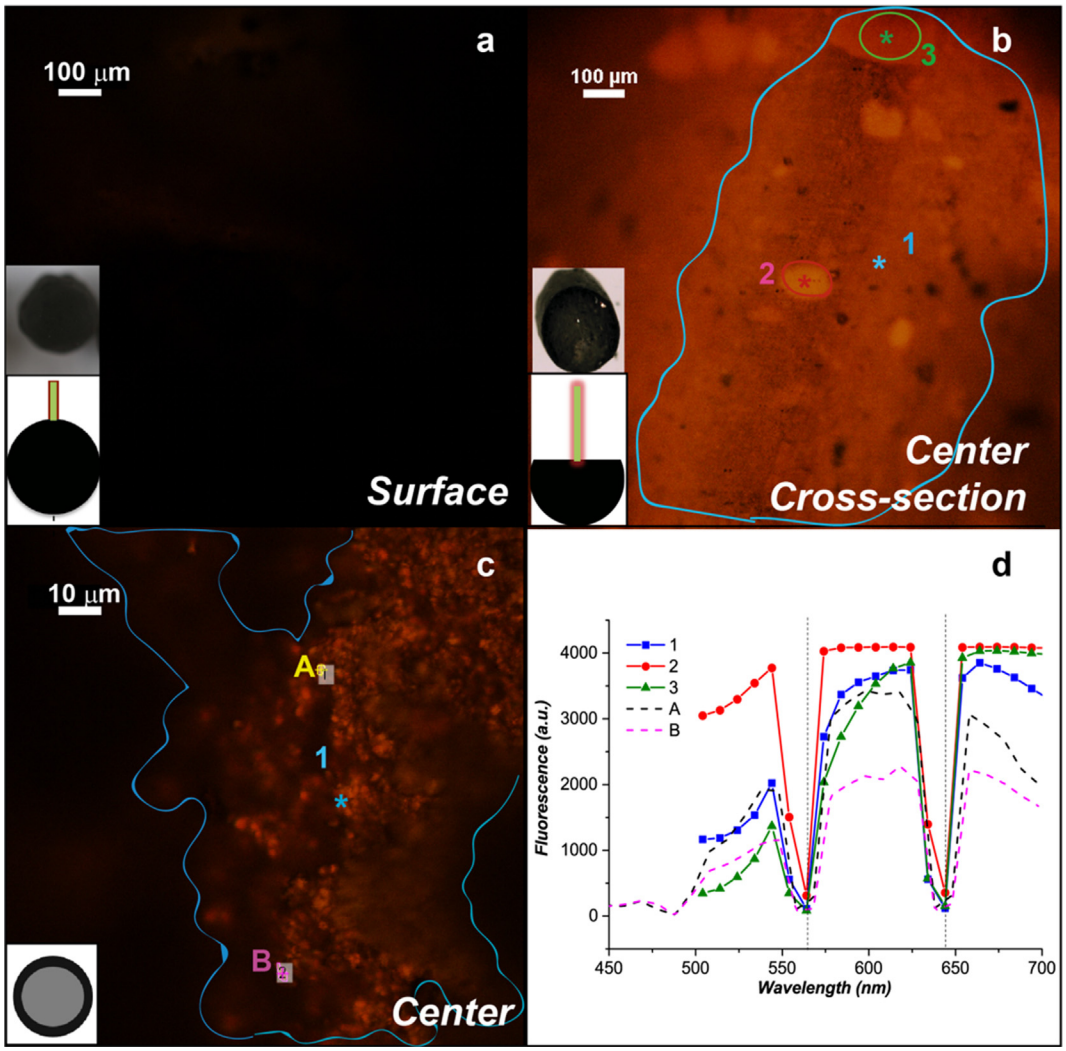

Fig. 2. Confocal fluorescence microscopy (CFM) images of the spent ZrO_2/ds-ZSM-5-ATP catalyst extrudate. Top: 10 times magnification of surface (a) and center of the cross-section of the technical catalyst (b). Bottom: 100 times magnification of center of the cross-section (c) and corresponding spectral information for the regions of interest indicated. Dashed vertical lines represent the excitation lasers, which are fixed at λ = 488, 561 and 642 nm. Insets in each image show photographs and schematic representations of irradiation on surface and cross-section.

The textural properties of the K-(USY-ATP) catalyst extrudate were severely affected upon cascaded bio-oil deoxygenation. The isotherm for the spent catalyst sample revealed a substantial loss in micro- and mesopore volume (black series Fig. S5c). BJH analysis derived from pore-size distribution plot (Fig. S5d) confirmed that the mesopores were partially shuttered after reaction. Besides, an important loss in surface area after reaction was noted too. The affected textural properties were partially restored upon regeneration, as the improved values of micro- and mesoporosity and BET indicate, but to a much lesser extent than with the zeolite ZSM-5-based catalyst material.

3.2.4. Changes in acidity

The acidity of fresh, spent and regenerated catalysts was assessed by FT-IR spectroscopy with pyridine as probe molecule.

The Brønsted acid sites (BAS) of the ZrO_2/ds-ZSM-5-ATP catalyst originate from the zeolite component [51] and are indicated by the 1545 and 1636 cm^{-1} bands in Fig. 3a [59,60]); the Lewis acid sites (LAS) come from the acidic Al^{3+} ions (indicated by the bands at 1455 and 1620 cm^{-1} [59–62]), the Zr^{4+} from the ZrO_2 component, and from different cations within the attapulgite (e.g., $Fe^{2+/3+}$, Mg^{2+}, Ca^{2+} [62,63] indicated by the multiple bands in the range 1443–1455 cm^{-1}. Quantification of the BAS was based on the integration of the 1545 cm^{-1} band -for fresh, spent and regenerated catalysts- while the ca. 1448 cm^{-1} band was used for determining the LAS [61]. After ex-situ CFP reaction the overall acidity (BAS + LAS) of the ZrO_2/ds-ZSM-5-ATP catalyst dropped significantly, being specially affected the strong sites (~75% drop) (Fig. 3b, Fig. S6a). This may indicate that the strong Lewis and Brønsted acid sites are the main contributors to the catalyst activity and that deactivation occurs due to site poisoning [53,54]. Indeed, the induced mesoporosity of the desilicated ZrO_2/ds-ZSM-5-ATP catalyst prevents from deactivation by pore occlusion [35,50]. Upon regeneration most but not all acidity could be recovered, however, being the strong acid sites those with better recoverability once combusted the bulky coke.

The LAS recovered less than the BAS (Fig. 3b) which might point at likely changes in the attapulgite cations and Zr after reaction and regeneration. Indeed, it should be noted that the band located at 1612 cm^{-1}, attributed to pyridine interacting with *cus* (coordinatively unsaturated sites) and Zr species [64,65] (Lewis acidity, PyL), was of considerably higher intensity for the fresh than for the regenerated catalyst material (Fig. S6b). However, when compared to the intensity of other cations interacting with pyridine –

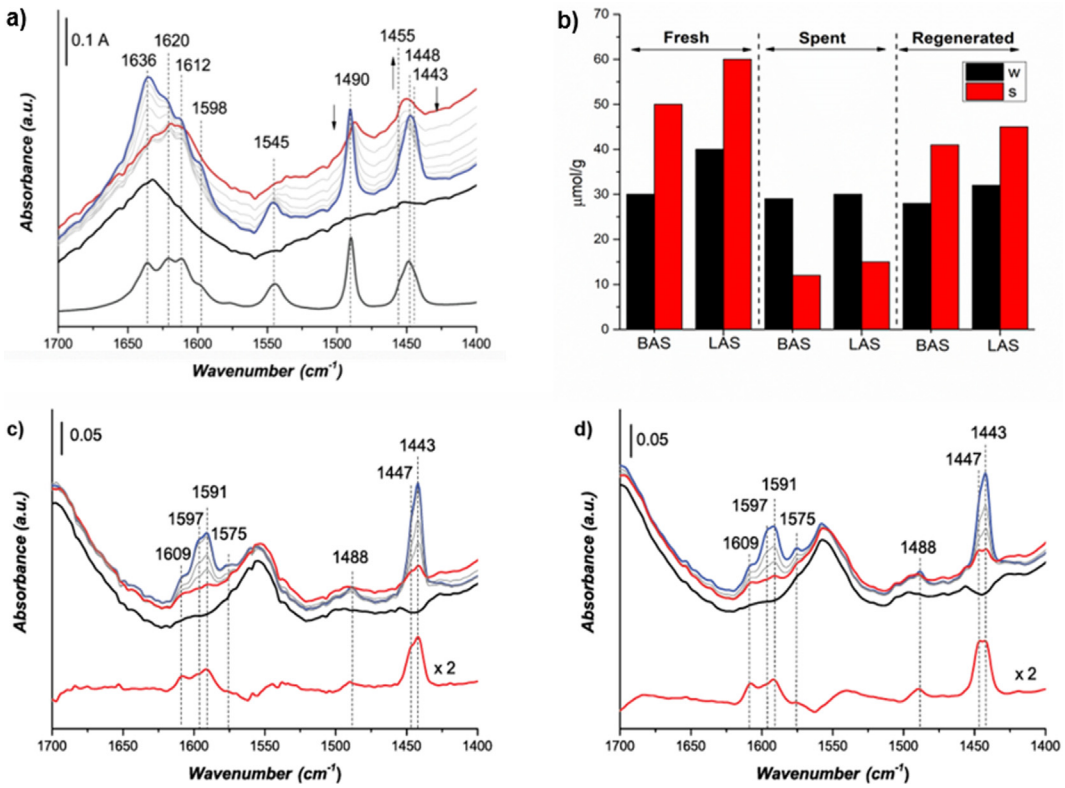

Fig. 3. a) Weight-normalized FT-IR spectroscopy of fresh ZrO_2/ds-ZSM-5-ATP and b) Quantification of weak (w, 150–250 °C) and strong (s, 350–450 °C) Brønsted (BAS) and Lewis acid sites (LAS) of fresh, spent and regenerated ZrO_2/ds-ZSM-5-ATP catalyst. (c–d) Weight-normalized FT-IR spectroscopy of fresh (c) and regenerated (d) K-(USY-ATP) catalysts during pyridine desorption from room temperature (blue) to 400 °C (red). The spectrum before pyridine exposure is marked in black. The off-set spectrum in grey corresponds to the background-corrected desorption spectrum taken at 150 °C. (For interpretation of the references to color in this figure legend, the reader is referred to the web version of this article.)

i.e., band at 1620 cm^{-1}- the relative intensity of PyL-Zr was larger for the regenerated than for the fresh catalyst material. This stronger PyL-Zr interaction is in line with the predicted ZrO_2 redispersion after reaction and regeneration.

Pyridine FT-IR studies showed the very limited acidity of the K-(USY-ATP) catalyst in line with its high Si/Al ratio (∼400). Yet the bands at 1443 cm^{-1} (attributed to pyridine adsorbed onto Lewis acidic K^+ cations [61,66]) and 1447 cm^{-1} (attributed to pyridine adsorbed onto a smaller cation present in the attapulgite, such as Al^{3+}, Fe^{3+}, Mg^{2+} and Ca^{2+}) [56] showed the presence of weak LAS, which disappeared after outgassing at 150 °C [61] (Fig. 3c). Upon cascaded bio-oil upgrading and regeneration was observed a good recovery of the sites within the attapulgite clay (indicated by the 1447 cm^{-1} band, see Fig. 3d). Quantification of the weak LAS, by integration of the 1447 and 1443 cm^{-1} bands, revealed that the total concentration was very low for the fresh and regenerated samples (Table 1). However, the bands attributed to K^+ (1443 cm^{-1}) lost their intensity, indicating some relocation or partial loss after reaction and regeneration. Note that K^+-sites, located in the sodalite cages of the FAU structure [15,56], would be significantly hindered/blocked in case structural damage occurs.

3.2.5. Changes in basicity

While acidity is the key to activity in catalytic pyrolysis, basicity is so for carrying out bio-oil deoxygenation. Bulk basicity of fresh, spent and regenerated K-(USY-ATP) catalyst extrudates was determined by CO_2-TPD and summarized in Table 1. After performing the catalytic reaction, a decrease of 70% in the number of basic sites was quantified. This dramatic basicity drop might be likely due to the consumption of basic OH groups during reaction (note that the FT-IR spectra of the spent catalyst in Fig. S2c did not show the characteristic stretching band O-H) and to structural damaging [18]. In line with the latter, oxygen vacancies might get clogged and K-OH sites (located in the sodalite cages of the USY zeolite [15,56]) inaccessible.

Rather than being recovered after regeneration, basicity dropped further due to likely zeolite structural damage suffered from the gases/steam generated by coke burning. Besides, the attapulgite phase may have been altered upon regeneration, getting affected oxygen anchoring to its basic sites in the form of alkaline cations (such as Mg^{2+}, Ca^{2+} and K^+ [56]).

3.2.6. Changes in structural properties

X-ray diffraction (XRD) was employed to measure the structural integrity of the fresh, spent and regenerated catalyst samples.

The orthorhombic phase of the zeolite ZSM-5 framework (Pnma space group, PDF 00-044-0003 [67]) remained well preserved after reaction (Fig. 4a-b). Nevertheless, the shape of some X-ray diffraction peaks changed a bit, including the transformation of the initially split peak at 2θ 26.8° and 27.1° into a single peak, and an intensity increase compared to the peak at 27.6° (Fig. 4b). These changes are typically attributed to the incorporation of organics within the zeolite framework [68,69]. A carbon phase (PDF 00-026-1077) assigned to graphitic coke can be tentatively identified in the XRD pattern of the spent catalyst sample at 2θ 31.5° [70–72], which is absent in the fresh sample. By contrast, the XRD peak seen at 31.0° (2θ) for the fresh sample and assigned to quartz, present as impurity in the binder [73], disappeared after catalysis. This is likely due to either a phase change of attapulgite, or agglomeration of phases due to sintering upon high temperatures.

The coke deposited during catalysis led to an increase in the ***b*** and ***c*** lattice parameters (Table 2) [69]. This was counterbalanced

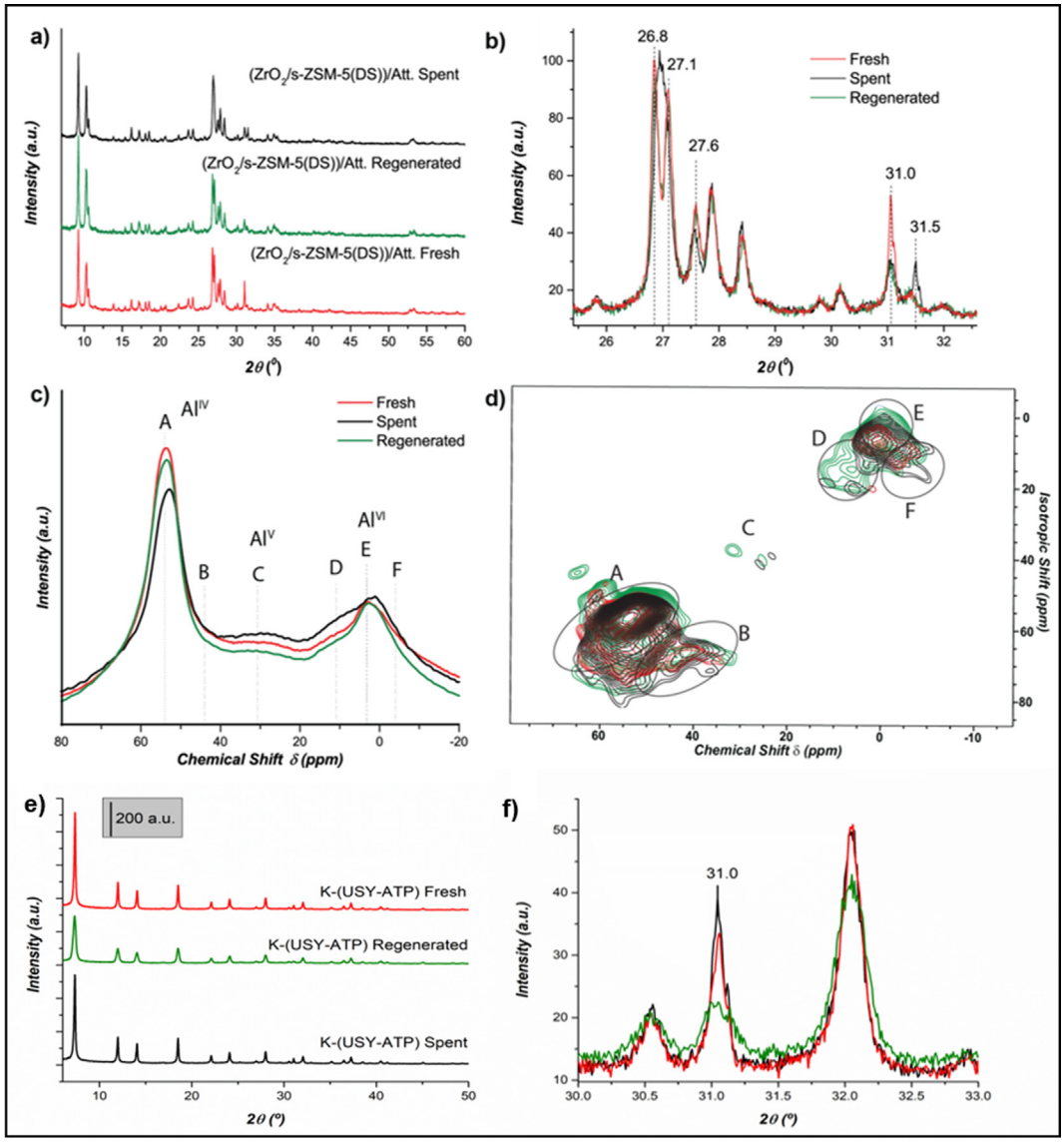

Fig. 4. (a–b) X-ray diffraction (XRD) patterns of the fresh (red), spent (black) and regenerated (green) ZrO_2/ds-ZSM-5-ATP catalyst materials at 2θ = 6–60° (a) and zoomed-in at 2θ = 26–32° (b). (c–d) ^{27}Al magic angle spinning (MAS) nuclear magnetic resonance (NMR) (c) and ^{27}Al MQ MAS NMR (d) spectra (deconvoluted in Fig. S7). (e–f) XRD patterns of the K-(USY-ATP) catalyst materials for the 2θ = 6–50° (e) and the 2θ = 30–33° (f) regions. (For interpretation of the references to color in this figure legend, the reader is referred to the web version of this article.)

by a contraction of the lattice parameter ***a***, likely related to slight dealumination [74], caused by contact with moisture coming from biomass vapors [75]. As response to these mild structural changes, it is observed a slight reduction of the crystal domain size, indicated by the decrease of the L_{VOL-IB} value in Table 2.

Upon regeneration, the original crystallite size was almost totally restored, as evidenced by a L_{VOL-IB} value close to the shown by the fresh sample (Table 2). The XRD pattern also showed the reappearance of the doublet peaks at (2θ) 26.8 and 27.1°, the original shape of the peak at 27.6°, together with the disappearance of the carbon phase at 31.5° (Fig. 4b). Regeneration resulted in lattice parameter changes opposite to those observed after reaction: ***b*** and ***c*** shortened, an indication of coke depletion, and ***a*** expanded back to the initial value of the fresh sample. The regeneration con-

Table 2
Lattice parameters values -a, b, c- and volume-weighted mean crystal domain size -L_{VOL-IB}- (determined using the Le Bail full-profile fit provided by the software Topas5) of the ZrO_2/ds-ZSM-5-ATP and K-(USY-ATP) catalytic materials, as determined by X-ray diffraction (XRD).

	Fresh	Spent	Regenerated	Fresh	Spent	Regenerated
Catalyst	ZrO_2/ds-ZSM-5-ATP			K-(USY-ATP)		
Space group	*Pnma*	*Pnma*	*Pnma*	*Fd-3m*	*Fd-3m*	*Fd-3m*
a (Å)	20.1278(6)	20.0794(6)	20.1278(6)	24.2704(5)	24.2579(4)	24.2434(8)
b (Å)	19.9364(5)	19.9529(6)	19.9405(6)	24.2704(5)	24.2579(4)	24.2434(8)
c (Å)	13.4038(5)	13.4099(5)	13.4033(5)	24.2704(5)	24.2579(4)	24.2434(8)
V_{cell} (Å)^3	5378.6(3)	5372.5(3)	5379.5(3)	14296.5(8)	14274.6(8)	14248.0(1)
L_{VOL-IB} (nm)	76.8(6)	70.7(6)	75.0(6)	62.6(3)	64.0(3)	30.1(1)

ditions, which expose the sample to high temperature and gas formation during the removal of coke deposits, could have possibly led to phase transformations of the attapulgite component. The absence of a quartz peak at 31.0° (2θ) in the regenerated sample indicates that the re-dispersion or phase change suffered upon reaction was irreversible. In addition, the unit cell size again increased in the regenerated sample, although the value of the fresh sample was not fully recovered.

Aluminum speciation in the fresh, spent and regenerated ZrO_2/ds-ZSM-5-ATP catalytic material has been assessed by ^{27}Al MAS (Fig. 4c) and ^{27}Al MQ MAS NMR (d) analyses. The main resonances of the fresh catalyst sample were located at 53 ppm (red series, Fig. 4c), assigned to framework tetrahedral coordinated Al species (A, Al^{IV}) [76,77], and at ca. 3 ppm, assigned to extra-framework octahedrally coordinated aluminum species (E, Al^{VI}) [78]. Interestingly, less well-defined extra-framework penta-coordinated Al (C, Al^{V}) species were also present for the fresh sample at ca. 30 ppm. After reaction the signal intensity of framework Al^{IV} species (so-called as A) decreased, in line with a loss in crystallinity, yet with concomitant signal increases in intensity of C and E at 30 ppm and 3 ppm, respectively (black series, c). Besides, the resonance of octahedral Al^{VI} species, E, shifted to a lower chemical shift. This change was better observed in the ^{27}Al MQ MAS NMR spectra (d) and believed to be related to distortions caused by pore coverage by coke [79]. In addition to the shift towards higher field, a shoulder emerged at 10 ppm (D, $Al^{VI'}$) (Fig. 4c), also attributed to broadening/structural distortions suffered upon coke build-up at high reaction temperature [74–76] (see expansion of D in Fig. 4d).

The acquired NMR spectra were fitted according to the different resonances identified (A → F) (Fig. S7) and the areas of the main deconvoluted spectra of the fresh, spent and regenerated catalyst samples were integrated to estimate the ratio between framework and extra-framework Al species (Table S1). The apparent drop of quantified framework Al sites after reaction is in line with the drop in Brønsted acidity noted above [76,80]. Yet, after catalyst regeneration, most of these Al sites seemed to be restored -as indicated by the increased intensity of A (green spectrum in Fig. 4c)-, recovering the framework tetrahedral coordination lost upon reaction. The signal associated with extra-framework Al^{VI} species, E, returned to its initial frequency position (c), while a large downfield distortion of signal D was noted. The increase in distortion of the Al^{VI} species after regeneration compared to the spent sample is likely associated with re-arrangement processes [81,82] of the attapulgite binder material during the thermal treatment, as a result of the gases/steam created upon coke burning. However, the overall ratio between framework and extra-framework Al was notably recovered, as shown in Table S1.

The XRD pattern of the K-(USY-ATP) catalyst material (red series, Fig. 4e-f) show the typical cubic pattern of the FAU phase of zeolite USY (PDF 00-045-0112) (see Table S2). As noted above, the diffraction peak observed at ca. 2θ = 31.0° (b) corresponds to the hexagonal phase of quartz (PDF 01-089-1961) [67], present as impurity in the attapulgite clay.

No meaningful structural changes are observed for the spent K-(USY-ATP) catalyst (black series in Fig. 4e). Contrarily to what observed for ZrO_2/ds-ZSM-5-ATP, no diffraction peak assigned to carbon was seen at 2θ = 31.5° for spent K-(USY-ATP) (black series), pointing at a more amorphous nature of coke.

The XRD pattern of the regenerated sample (green series) did show considerable changes regarding the fresh and spent catalysts patterns, such as the lower intensity and the overall broader peak widths. These may be an indication of a drop in crystallinity, compared to the fresh and spent samples. Indeed, significant unit cell shrinkage and reduced size of the crystalline domains (nearly by half) were confirmed upon estimation of the lattice parameters and crystallite sizes (V_{cell} and L_{VOL-IB} values, respectively, in Table 2). This decrease in crystallinity may have been provoked by the high temperature and the steam formed during coke burning upon catalyst regeneration, likely provoking hydrolysis of the grafted K species (Si—O—K^+ + H_2O → Si—OH + KOH), and ultimately loss of the catalyst's basicity. Although smaller these ca. 30 nm crystals do keep their structural properties to a great extent; otherwise, a dramatic decrease of the textural properties would have been observed.

3.2.7. Changes in morphology

When examining the morphology of the ZrO_2/ds-ZSM-5-ATP catalyst no significant changes were seen after reaction and regeneration compared to fresh samples. Scanning electron microscopy (SEM) and transmission electron microscopy (TEM) images, which are shown in Fig. S8, reveal well-preserved zeolite ZSM-5 grains (of ca. 0.5–2 μm) agglomerated within 4 to 10 μm particles, and embraced by needle-like agglomerates of attapulgite (0.5 μm × 30 nm), accumulating more on edges and surface zeolite defects. Note that quartz impurities [73,83] were detected in the attapulgite in fresh (f) and regenerated samples (h). The TEM images show segregated domains of binder and zeolite, of varied sizes and shapes, unaltered after reaction and regeneration (Fig. S8c-h). Yet, a likely presence of coke-derived carbon flakes [75] were observed in TEM images of the spent catalyst, deposited on the edges of the zeolite crystal (left side Fig. S8g). Also, a high magnification TEM image of the fresh ZrO_2/ds-ZSM-5-ATP catalyst (Fig. S8f) revealed the presence of nanosized ZrO_2 particles distributed on the zeolite crystals where this component was originally deposited via impregnation, but also on the attapulgite clay binder material. This observation could indicate that ZrO_2 was re-dispersed during granulation and calcination. Furthermore, ZrO_2 might have re-dispersed after regeneration, as illustrated by the aggregated clusters formed onto the regenerated ZrO_2/ds-ZSM-5-ATP catalyst (Fig. S8h).

Re-dispersion effects were further studied by μ-XRF (Fig. 5a-b). On the fresh catalyst body (a) can be seen that Zr species preferably remained close to zeolite domains. It should be noted that zeolite domains are easily identified by the higher presence of Si -predominant in the zeolite- and in particular by the absence of a Mg signal which is unique for the attapulgite clay. On the contrary, Zr species seem to re-disperse upon reaction and regeneration, as indicated by the Zr signal of the regenerated catalyst body (Fig. 5b) which is also detected at the attapulgite domains.

SEM (Fig. S9) and TEM images (Fig. 5c,f) of the fresh K-(USY-ATP) catalyst material showed particle sizes of 300–500 nm. Attapulgite aggregates, identified by its characteristic needle-like morphology, were found on the zeolite crystal edges. Compared to the fresh sample, the zeolite particles seemed irreversibly clustered and of smaller size after reaction (d,g) and regeneration (e,h), in support of the structural modification noted above.

In the high magnification image of the fresh catalyst (Fig. 5f) mesopores -generated via dealumination- with dimensions of ca. 20 nm can be distinguished. These were not observed with any clarity in the spent catalyst (g), however, presumably due to coverage by coke deposits. In the case of the regenerated sample (h), cavities can be seen, likely created by interconnection of mesopores [84].

4. Discussion

4.1. Catalytic pyrolysis

Upon *ex-situ* CFP, the ZrO_2/ds-ZSM-5-ATP catalyst developed coke consisting of highly polyaromatic deposits, as indicated by TGA-MS, FT-IR and UV–Vis DRS. Confocal fluorescence microscopy mapping showed that the coke deposits are distributed heteroge-

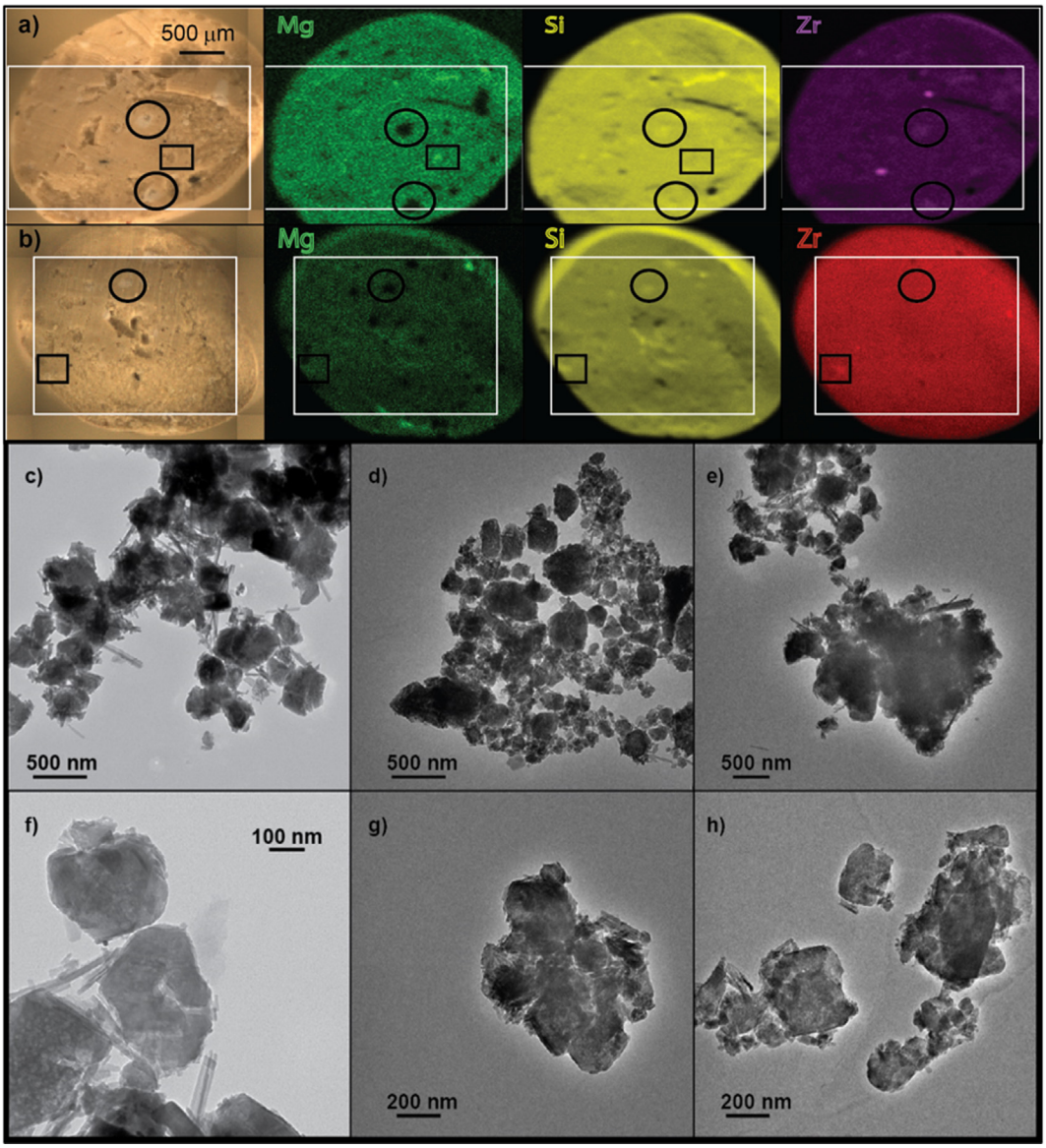

Fig. 5. (a–b) Mounted images of the ZrO_2/ds-ZSM-5-ATP fresh (a) and regenerated (b) catalyst bodies with the corresponding elemental mappings obtained by μ-X-ray fluorescence (XRF). White rectangles indicate the zone analyzed within the same scanned plane; small circles and squares indicate regions of interest mentioned in the text. (c–h) Representative transmission electron microscopy (TEM) images of the (c,f) fresh, (d,g) spent, and (e,h) regenerated K-(USY-ATP) catalyst materials.

neously, i.e., with an egg-shell pattern, over the technical catalyst: being more poly-aromatic and abundant on the surface, and its concentration diminishing progressively towards the inside of the body. By applying Raman spectroscopy, the soluble fraction of coke was estimated to range between 5 and 10 Å in size. These large coke species locate in the zeolite's mesopores, partially blocking the strong acid sites, but also form externally, affecting the catalyst's textural properties too. This was demonstrated with Ar physisorption and py-FT-IR spectroscopy, which showed drops in both (meso)pore volume, surface area and acidity, thereby especially affecting the strong (and Lewis and Brønsted) acid sites. Coke deposition also led to structural changes, as observed by XRD with the expansion of the lattice parameters.

Another structural change pointed out by XRD is the re-distribution/phase change of attapulgite, evidenced by the observed contraction of the unit cell of the ZrO_2/ds-ZSM-5-ATP catalyst after reaction. Such a change was also observed in the ^{27}Al MAS NMR spectra, which showed an enhancement of the EFAl species in the spent catalyst at the expense of the tetracoordinated framework Al species. Penta- and, in particular octahedral Al species, increased in amount and extension, i.e., broadened, suggesting relocations upon catalytic reaction. No significant morphological changes were seen in the TEM images of the spent sample.

Regeneration, carried out in static air for 6 h at 550 °C to burn-off the coke deposits, efficiently restored the textural properties and acidity previously affected by the formed coke, ruling-out any significant structural collapse. TNH_3-TPD and FT-IR spectroscopy with pyridine as probe molecule did, however, confirm some irreversible loss in the acidity for the regenerated catalyst material. FT-IR also showed a relative larger intensity of the PyL-Zr band for the regenerated catalyst relative to the fresh catalyst, which suggests ZrO_2 re-dispersion, as confirmed by μ-XRF.

The ^{27}Al MAS NMR measurements indicate that the distortions created after regeneration are more pronounced than after reaction, likely due to re-arrangement processes of the attapulgite as a result of the gas/steam created under the regeneration conditions. Structural changes after regeneration were also observed by XRD, as indicated by the disappearance of the quartz impurity

in the attapulgite binder. Despite some distortion of the EFAl species, the framework Al species were mostly recuperated. The attapulgite phase is believed to play an important role in this regeneration given its high content in SiO_2 and Al_2O_3, which serve as reservoir upon Al distortion effects suffered during reaction.

4.2. Cascaded catalytic deoxygenation

After bio-oil upgrading the K-(USY-ATP) catalyst extrudates suffered structural damage and pore blockage by coke. It was determined by TGA-MS, FT-IR, UV–Vis DRS and confocal fluorescence microscopy that the coke deposits consisted of a large proportion of naphthalenes/anthracenes and poly-aromatics, distributed again in an egg-shell manner over the spent catalyst extrudate. However, these coke deposits were of a softer nature (i.e. H-richer) than the coke deposits formed on the ZrO_2/ds-ZSM-5-ATP catalyst used for the catalytic fast pyrolysis stage. This is in line with the latter being upstream and directly exposed to the crude pyrolysis vapors, while the K-USY-based catalyst further upgrades the already treated vapors. Another factor for which less poly-aromatic coke formed onto the K-USY-Attapulgite catalyst is the lack of strong acid sites where it develops more easily. The textural properties of the spent catalyst nevertheless were severely affected by coke formation and morphological damages, as determined by physisorption and TEM measurements. The observed clustering had detrimental consequences for the required basicity of the catalyst material, as determined by CO_2-TPD, by means of clogged oxygen vacancies or hindering accessibility to the K^+ and OH^- sites.

Loss of structural integrity was enhanced upon catalyst regeneration due to the steam formed during coke burning, with the complete loss of basic sites. XRD measurements revealed the shrinkage of the zeolite unit-cell as well as a loss of crystallite size in the regenerated catalyst. The original textural properties, affected by coke deposition and regeneration, could only be partially recovered, less so than with the CFP catalyst. The Py-FT-IR spectroscopy studies indeed suggested some loss in K-loading after reaction and/or regeneration. The changes in physicochemical properties correlated with the morphological changes, as observed by TEM, for the zeolite material regenerated.

5. Conclusions

A cascade process, consisting of a thermal pyrolysis followed by a two-step catalytic *ex-situ* catalytic fast pyrolysis (CFP) -catalyzed by a ZrO_2/desilicated zeolite ZSM-5-/attapulgite material as solid acid- and the subsequent catalytic upgrading/deoxygenation of the formed oil -catalyzed by a K-(zeolite USY-attapulgite) material as solid base- was studied for the production of bio-oil from lignocellulosic biomass. A high bio-oil mass yield was achieved (40 wt%) with a remarkable deoxygenation degree (60 wt%), compared to a non-catalytic thermal bio-oil.

Upon *ex-situ* CFP the solid acid ZrO_2/desilicated zeolite ZSM-5-attapulgite catalyst suffers acid site coverage by the build-up of coke deposits and (reversible) changes in the Al coordination. In the case of the base K-(zeolite USY-attapulgite) catalyst, employed to further upgrade the formed bio-oil via CFP, mild pore blockage by coke formation and a partial loss of structural integrity was observed. Yet, the main deactivation cause is ascribed to clustering of the crystallites which hinders the catalyst's basicity.

Regeneration of the deactivated catalysts by coke burn-off to a large extent reverted the negative effects of the coke deposition on the ZrO_2/desilicated zeolite ZSM-5-attapulgite catalyst. Although the structural distortion suffered by the catalyst upon pyrolysis can be considered mild and reversible, the small losses in framework Al and acidity upon a complete reaction plus regeneration cycle will progressively attenuate its activity. This, together with the observed ZrO_2 migration after reaction and regeneration will eventually require catalyst replacement by fresh material after few reaction cycles.

In contrast, the regeneration procedure caused irreversible structural change in the K-(zeolite USY-attapulgite) catalyst. It is believed that the steam produced upon coke burning provokes hydrolysis of the grafted K species, with the KOH produced attacking the zeolite's structure, which ultimately experiences a total loss of basicity. This implies that after only one reaction cycle the K-(zeolite USY-attapulgite) catalyst would need to be replaced, with its associated economic implications for the process.

Alternative regeneration procedures which efficiently restore the initial properties of the alkaline-exchanged USY catalyst material or the revision of the grafting procedure which, as seen, negatively impacts on the structure of the catalyst in the downstream process, might offer an alternative here. Among them, performing the regeneration at milder temperature conditions and in a flow reactor rather in a muffle furnace at static conditions would shorten the long exposure of the catalyst to the produced water vapors upon coke combustion, likely preventing structural damage and basicity loss. Also, to correct for hindered basicity a newly alkaline grafting process could be accomplished after regeneration, replenishing the extinguished K-OH sites. Testing of these newly proposed recoverability methods and the determination of the catalysts' lifespans, i.e., the number of regeneration cycles that the catalysts can survive before getting replaced, could be topics for future investigation.

Declaration of Competing Interest

The authors declare that they have no known competing financial interests or personal relationships that could have appeared to influence the work reported in this paper.

Acknowledgements

Authors gratefully acknowledge the financial support from the European Union Seventh Framework Programme (FP7/ 2007-2013) under grant agreement n°604307 (CASCATBEL project). Dr. T. Hartman (Utrecht University, UU) is thanked for recording the Raman spectra, while Dr. A.-E. Nieuwelink (UU) is acknowledged for performing the μ-XRF analysis. The NMR experiments were supported by the Netherlands Organization for Scientific Research (NWO) within the Middelgroot program (no. 700.58.102 to M.B.), and uNMR-NL, an NWO-funded National Roadmap Large-Scale Facility for The Netherlands (no. 184.032.207).

Authors contributions

A.M.H.G. contributed to the idea of this study, conducted experimental work, processed the results and wrote the manuscript. R. M.D. and E.T.C.V. calculated the XRD lattice parameters, interpreting the results. H.H. and D.P.S. run the catalytic tests and participated in the interpretation of the results. K.H. and M. B. performed the ^{27}Al (MQ) MAS NMR measurements. P.C.A.B. contributed to the idea of this work and aided on the discussion of results and manuscript writing. B.M.W. contributed to the idea of this study, including manuscript design and writing.

Appendix A. Supplementary material

Supplementary data to this article can be found online at https://doi.org/10.1016/j.jcat.2021.09.029.

References

[1] W.N.R.W. Isahak, M.W.M. Hisham, M.A. Yarmo, T.Y. Yun Hin, Renew. Sustain. Energy Rev. 16 (2012) 5910.
[2] U.S.M. Bertero, G. de la Puente, Fuel 95 (2012) 263.
[3] R. French, S. Czernik, Fuel Process. Technol. 91 (2010) 25.
[4] K. Wang, P.A. Johnston, R.C. Brown, Bioresour. Technol. 173 (2015) 124.
[5] H. Zhang, S. Shao, R. Xiao, D. Shen, J. Zeng, Energy Fuels 28 (2014) 52.
[6] C. Liu, H. Wang, A.M. Karim, J. Sun, Y. Wang, Chem. Soc. Rev. 43 (2014) 7594.
[7] M.M. Yung, A.K. Starace, C. Mukarakate, A.M. Crow, M.A. Leshnov, K.A. Magrini, Energy Fuels 30 (2016) 5259.
[8] M.M. Yung, A.R. Stanton, K. Iisa, R. French, K.A. Orton, K.A. Magrini, Energy Fuels 30 (2016) 9471.
[9] D. Verboekend, J. Pérez-Ramírez, Catal. Sci. Technol. 1 (2011) 879.
[10] J. Gou, Z. Wang, C. Li, X. Qi, V. Vattipalli, Y.-T. Cheng, G. Huber, W.C. Conner, P.J. Dauenhauer, T.J. Mountziaris, W. Fan, Green Chem. 19 (2017) 3549.
[11] P.S. Rezaei, H. Shafaghat, W.M.A.W. Daud, Appl. Catal. A: General 469 (2014) 490.
[12] G. Pacchioni, ACS Catal. 4 (2014) 2874.
[13] A. Osatiashtiani, B. Puértolas, C.C.S. Oliveira, J.C. Manayil, B. Barbero, M. Isaacs, C. Michailof, E. Heracleous, J. Pérez-Ramírez, A.F. Lee, K. Wilson, Biomass Convers. Biorefin. 7 (2017) 331.
[14] B. Puértolas, T.C. Keller, S. Mitchell, J. Pérez-Ramírez, Appl. Catal. B: Environ. 184 (2016) 77.
[15] A.M. Hernández-Giménez, J. Ruiz-Martínez, B. Puértolas, J. Pérez-Ramírez, P.C. A. Bruijnincx, B.M. Weckhuysen, Top. Catal. 60 (2017) 1522.
[16] A. Oasmaa, A. Källi, C. Lindfors, D.C. Elliott, D. Springer, C. Peacocke, D. Chiaramonti, Energy Fuels 26 (2012) 3864.
[17] H. Hattori, Chem. Rev. 95 (1995) 537.
[18] T.C. Keller, K. Desai, S. Mitchell, J. Pérez-Ramírez, ACS Catal. 5 (2015) 5388.
[19] S. Mitchell, N.-L. Michels, K. Kunze, J. Pérez-Ramírez, Nat. Chem. 4 (2012) 825.
[20] R.V. Jasra, B. Tyagi, Y.M. Badheka, V.N. Choudary, T.S.G. Bhat, Ind. Eng. Chem. Res. 42 (2003) 3263.
[21] M.A. Uguina, J.L. Sotelo, D.P. Serrano, Appl. Catal. 76 (1991) 183.
[22] E.T.C. Vogt, G.T. Whiting, A. Dutta Chowdhury, B.M. Weckhuysen, Adv. Catal. 58 (2015) 143.
[23] E.T.C. Vogt, B.M. Weckhuysen, Chem. Soc. Rev. 44 (2015) 7342.
[24] P. Gélin, T. Des Courières, Appl. Catal. 72 (1991) 179.
[25] H.S. Cerqueira, G. Caeiro, L. Costa, F. Ramôa Ribeiro, J. Mol. Catal. A: Chem. 292 (2008) 1.
[26] Á. Ibarra, A. Veloso, J. Bilbao, J.M. Arandes, P. Castaño, Appl. Catal. B 182 (2016) 336.
[27] F. Meirer, S. Kalirai, J.N. Weker, Y. Liu, J.C. Andrews, B.M. Weckhuysen, Chem. Commun. 51 (2015) 8097.
[28] F. Meirer, D.T. Morris, S. Kalirai, Y. Liu, J.C. Andrews, B.M. Weckhuysen, J. Am. Chem. Soc. 137 (2015) 102.
[29] F. Meirer, S. Kalirai, D. Morris, S. Soparawalla, Y. Liu, G. Mesu, J.C. Andrews, B. M. Weckhuysen, Sci. Adv. 1 (2015) e1400199.
[30] S.P. Verkleij, G.T. Whiting, S. Parres-Esclapez, S. Li, M.M. Mertens, A.J. Bons, M. Burgers, B.M. Weckhuysen, Catal. Sci. Technol. 8 (2018) 2175.
[31] S.P. Verkleij, G.T. Whiting, D. Pieper, S. Parres-Esclapez, S. Li, M.M. Mertens, M. Janssen, A.J. Bons, M. Burgers, B.M. Weckhuysen, ChemCatChem 11 (2019) 4788.
[32] S.P. Verkleij, G.T. Whiting, S. Parres-Esclapez, S. Li, M.M. Mertens, M. Janssen, A. J. Bons, M. Burgers, B.M. Weckhuysen, ChemCatChem 12 (2020) 5465.
[33] A.M. Hernández-Giménez, E. Heracleous, E. Pachatoudirou, A. Horvat, H. Hernando, D.P. Serrano, A.A. Lappas, P.C.A. Bruijnincx, B.M. Weckhuysen, ChemCatChem 13 (2020) 1207.
[34] M. Guisnet, P. Magnoux, Catal. Today 36 (1987) 477.
[35] F. Schmidt, C. Hoffman, G. Filippo, S. Bordiga, P. Simon, W. Carrill-Cabrera, S. Kaskel, J. Catal. 307 (2013) 238.
[36] N.L. Michels, S. Mitchell, J. Pérez-Ramírez, ACS Catal. 4 (2014) 2409.
[37] E. Heracleous, E. Pachatouridou, A.M. Hernández-Giménez, H. Hernando, T. Fakin, A.L. Paioni, M. Baldus, D.P. Serrano, P.C.A. Bruijnincx, B.M. Weckhuysen, A.A. Lappas, J. Catal. 380 (2019) 108.
[38] H. Hernando, B. Puértolas, P. Pizarro, J. Fermoso, J. Pérez-Ramírez, D.P. Serrano, ACS Sustain. Chem. Eng. 7 (2019) 18027.
[39] J. Fermoso, H. Hernando, S. Jiménez-Sánchez, A.A. Lappas, E. Heracleous, P. Pizarro, J.M. Coronado, D.P. Serrano, Fuel Process. Technol. 167 (2017) 563.
[40] M. Guisnet, P. Magnoux, Appl. Catal. A: General 212 (2001) 83.
[41] H.G. Karge, W. Nießen, H. Bludau, Appl. Catal. A: General 146 (1996) 339.
[42] S.U. Kulkarni, W.P. Hoffman, M.C. Thies, Carbon 59 (2013) 33.
[43] P.S. Kalsi, Spectroscopy of Organic Compounds, sixth ed., New Age International Publishers, New Delhi, 2004, p. 9.
[44] A.C. Ferrari, J. Robertson, Philos. Trans. A. Math. Phys. Eng. Sci. 362 (2004) 2477.
[45] A.C. Ferrari, Solid State Commun. 143 (2007) 47.
[46] M. Guisnet, P. Magnoux, Appl. Catal. 54 (1989) 1.
[47] A.N. Parvulescu, D. Mores, E. Stavitski, C.M. Teodorescu, P.C.A. Bruijnincx, R.J. M.K. Gebbink, B.M. Weckhuysen, J. Am. Chem. Soc. 132 (2010) 10429.
[48] D. Mores, J. Kornatowski, U. Olsbye, B.M. Weckhuysen, Chem. Eur. J. 17 (2011) 2874.
[49] A.S. Al-Dughaither, H. De Lasa, Ind. Eng. Chem. Res. 53 (2014) 15303.
[50] S. Bordiga, C. Lamberti, F. Bonino, A. Travert, F. Thibault-Starzyk, Chem. Soc. Rev. 44 (2015) 7262.
[51] H. Hernando, A.M. Hernández-Giménez, C. Ochoa-Hernández, P.C.A. Bruijnincx, K. Houben, M. Baldus, P. Pizarro, J.M. Coronado, J. Fermoso, J. Čejkac, B.M. Weckhuysen, D.P. Serrano, Green Chem. 20 (2018) 3499.
[52] H. Hernando, A.M. Hernández-Giménez, S. Gutiérrez-Rubio, T. Fakin, A. Horvat, R.M. Danisi, P. Pizarro, J. Fermoso, E. Heracleous, P.C.A. Bruijnincx, A.A. Lappas, B.M. Weckhuysen, D.P. Serrano, ChemSusChem 12 (2019) 2428.
[53] M. Guisnet, P. Magnoux, D. Martin, Stud. Surf. Sci. Catal. 111 (1997) 1.
[54] N. Katada, M. Niwa, Catal. Surv. Asia 8 (2004) 161.
[55] E.C. Nordvang, E. Borodina, J. Ruiz-Martínez, R. Fehrmann, B.M. Weckhuysen, Chem. Eur. J. 21 (2015) 17324.
[56] A.M. Hernández-Giménez, L.M. de Kort, G.T. Whiting, H. Hernando, B. Puértolas, J. Pérez-Ramírez, D.P. Serrano, P.C.A. Bruijnincx, B.M. Weckhuysen, ChemCatChem 13 (2021) 1951.
[57] K.S.W. Sing, D.H. Everett, R.A.W. Haul, L. Moscou, R.A. Pierotti, J. Rouquerol, Pure Appl. Chem. 57 (1985) 603.
[58] K.S.W. Sing, R.T. Williams, Adsorpt. Sci. Technol. 22 (2004) 773.
[59] V. Rac, V. Rakic, D. Stocic, O. Otman, A. Auroux, Microporous Mesoporous Mater. 194 (2014) 126.
[60] D.P. Serrano, R.A. García, G. Vicente, M. Linares, D. Procházková, J. Čejka, J. Catal. 279 (2011) 366.
[61] C.A. Emeis, J. Catal. 141 (1993) 347.
[62] C. Li, Z. Wu, in: Handbook of Zeolite Science and Technology, Marcel Dekker, New York, 2011, p. 541.
[63] S.H. Begum, C. Te Hung, Y.T. Chen, S.J. Huang, P.H. Wu, X. Han, S. Bin Liu, J. Mol. Catal. A: Chemical 423 (2016) 423.
[64] K. Hadjiivanov, Adv. Catal. 57 (2014) 99.
[65] I.M. Hill, S. Hanspal, Z.D. Young, R.J. Davis, J. Phys. Chem. C 119 (2015) 9186.
[66] A. Guzmán, I. Zuazo, A. Feller, R. Olindo, C. Sievers, J.A. Lercher, Microporous Mesoporous Mater. 83 (2005) 309.
[67] M.M. Treacy, J.B. Higgins, Collection of Simulated XRD Powder Patterns for Zeolites, fifth ed., Elsevier, Amsterdam, 2007, p. 184.
[68] E.L. Wu, S.L. Lawton, D.H. Olson, A.C. Rohrman, G.T. Kokotailo, J. Phys. Chem. 83 (1979) 2777.
[69] A.G. Álvarez, H. Viturro, R.D. Bonetto, Mater. Chem. Phys. 32 (1992) 135.
[70] J.M. Jiménez-Mateos, E. Romero, C. Gómez de Salazar, Carbon 31 (1993) 1159.
[71] F.R. Feret, Analyst 123 (1998) 595.
[72] L. Hong, S. Benxian, Energ. Source Part A 32 (2010) 1159.
[73] J. Zhang, X. Liu, Phys. Chem. Chem. Phys. 16 (2014) 8655.
[74] Y. García-Basabe, I. Rodríguez-Iznaga, L.C. de Menorval, P.L. Llewellyn, G. Maurin, D.W. Lewis, R. Binions, M. Autie, A.R. Ruiz-Salvador, Microporous Mesoporous Mater. 135 (2010) 187.
[75] Y. Fan, Y. Cai, X. Li, H. Yin, J. Xia, J. Ind. Eng. Chem. 46 (2017) 139.
[76] M. Hunger, in: Zeolite Characterization and Catalysis: A Tutorial, Springer, New York, 2010, p. 65.
[77] Z. Yan, D. Ma, J. Zhuang, X. Liu, X. Liu, X. Han, X. Bao, F. Chang, L. Xu, Z. Liu, J. Mol. Catal. A: Chem. 194 (2003) 153.
[78] J.A. van Bokhoven, N. Danilina, in J. Cejka, A. Corma, S. Zones (Eds.), Zeolites and Catalysis, Synthesis, Reactions and Applications, vol. 1, Wiley-VCH, Weinheim, 2010, pp. 283.
[79] A. Devaraj, M. Vijayakumar, J. Bao, M.F. Guo, M.A. Derewinski, Z. Xu, M.J. Gray, S. Prodinger, K.K. Ramasamy, Sci. Rep. 6 (2016) 37586.
[80] H.M. Kao, C.P. Grey, K. Pitchumani, P.H. Lakshminarasimhan, V. Ramamurthy, J. Phys. Chem. A 102 (1998) 5627.
[81] Y. Oumi, R. Mizuno, K. Azuma, S. Nawata, T. Fukushima, Microporous Mesoporous Mater. 49 (2011) 103.
[82] M.C. Silaghi, C. Chizallet, J. Sauer, P. Raybaud, J. Catal. 339 (2016) 242.
[83] L. Rodríguez-González, F. Hermes, M. Bertmer, E. Rodríguez-Castellón, A. Jiménez-López, U. Simon, Appl. Catal. A: General 328 (2007) 174.
[84] K.P. de Jong, J. Zecevic, H. Friedrich, P.E. de Jongh, M. Bulut, S. van Donk, R. Kenmogne, A. Finiels, V. Hulea, F. Fajula, Angew. Chem. Int. Ed. 49 (2010) 10074.